JACS
JOURNAL OF THE AMERICAN CHEMICAL SOCIETY
pubs.acs.org/JACS
Article

Hydrolysis-Based Small-Molecule Hydrogen Selenide (H_2Se) Donors for Intracellular H_2Se Delivery

Turner D. Newton, Sarah G. Bolton, Arman C. Garcia, Julie E. Chouinard, Stephen L. Golledge, Lev N. Zakharov, and Michael D. Pluth*

Cite This: J. Am. Chem. Soc. 2021, 143, 19542−19550
Read Online
ACCESS | Metrics & More | Article Recommendations | Supporting Information

ABSTRACT: Hydrogen selenide (H_2Se) is a central metabolite in the biological processing of selenium for incorporation into selenoproteins, which play crucial antioxidant roles in biological systems. Despite being integral to proper physiological function, this reactive selenium species (RSeS) has received limited attention. We recently reported an early example of a H_2Se donor (TDN1042) that exhibited slow, sustained release through hydrolysis. Here we expand that technology based on the P═Se motif to develop cyclic-PSe compounds with increased rates of hydrolysis and function through well-defined mechanisms as monitored by ^{31}P and ^{77}Se NMR spectroscopy. In addition, we report a colorimetric method based on the reaction of H_2Se with NBD-Cl to generate NBD-SeH (λ_{max} = 551 nm), which can be used to detect free H_2Se. Furthermore, we use TOF-SIMS (time of flight secondary ion mass spectroscopy) to demonstrate that these H_2Se donors are cell permeable and use this technique for spatial mapping of the intracellular Se content after H_2Se delivery. Moreover, these H_2Se donors reduce endogenous intracellular reactive oxygen species (ROS) levels. Taken together, this work expands the toolbox of H_2Se donor technology and sets the stage for future work focused on the biological activity and beneficial applications of H_2Se and related bioinorganic RSeS.

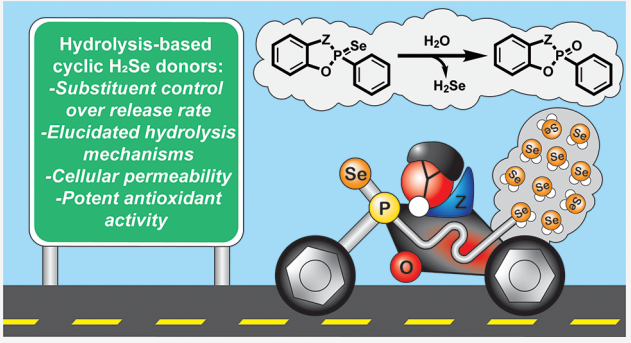

INTRODUCTION

Selenium is a trace nutrient that is required in the human diet for proper physiological function.[1−4] The biological concentration window for selenium is narrow, and dietary selenium deficiency or excess can lead to detrimental conditions including Keshan's disease[5] and selenosis.[6] Primary dietary sources of selenium include organoselenium compounds and inorganic salts,[7] both of which can be incorporated into selenoproteins through different transformations or excreted to prevent toxic accumulation.[8,9] One commonality between these major metabolic pathways is that they are thought to proceed through the intermediate formation of hydrogen selenide (H_2Se) (Figure 1). Drawing parallels to its lighter congener H_2S, H_2Se is highly reactive and toxic but also crucial for selenium homeostasis, proper function of endogenous antioxidant systems, and thyroid function.[10] Despite the importance of H_2Se and related reactive selenium species (RSeS), few chemical tools allow for direct delivery of these species to biological environments. For example, most investigations focused on the therapeutic benefits of selenium, especially in relation to various cancers, have used oxidized selenium sources, such as sodium selenite (Na_2SeO_3), as the selenium source.[11,12] Significant evidence, however, suggests that reduced RSeS, such as selenium-glutathione adducts,

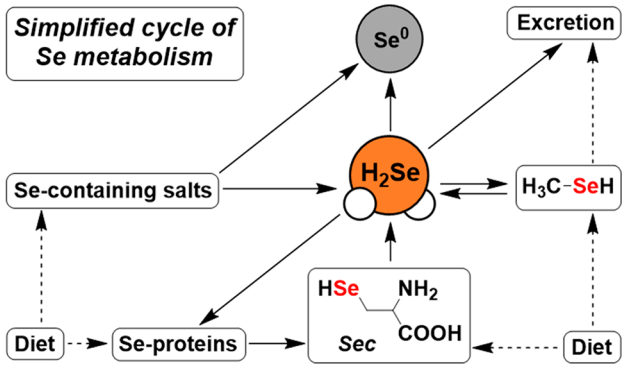

Figure 1. Simplified view of the selenium metabolic cycle highlighting the role of H_2Se in both protein synthesis and excretory pathways from dietary sources.

Received: September 8, 2021
Published: November 9, 2021

organoselenium species, or H_2Se, rather than oxidized Se species are responsible for observed *in vivo* activities.[13] For example, in a recent study by the Tang group, H_2Se was reported to be the active selenium metabolite responsible for cell death in HepG2 cells that were initially treated with Na_2SeO_3.[14] Similarly, Roth and co-workers found that direct administration of H_2Se, but not Na_2SeO_3, reduced heart damage in mouse models of myocardial ischemia reperfusion injury, suggesting that reduced RSeS exert different physiological effects from the more commonly used oxidized selenium sources.[15]

The blossoming interest in studying the chemical biology of H_2Se is reminiscent of the beginnings of contemporary research on biological H_2S. H_2S was classically recognized as a toxin but was later found to play essential roles in many key mammalian processes, including angiogenesis.[16] Sulfur and selenium are the most similar main group elements on the periodic table, and researchers are already proposing that H_2Se may be a fourth biological gasotransmitter, adding to the more commonly accepted H_2S, NO, and CO. Already meeting many of the criteria to be classified as a gasotransmitter, H_2Se is produced endogenously, is a gas in its diprotic state, is membrane permeable, and can exert unique biological effects although specific molecular targets in signaling pathways have not yet been identified.[17,18] When administered exogenously to mice through either inhalation (0−5 ppm in air) or injection (solution of NaSeH, 0.05−24.9 mg/kg), H_2Se modulates aerobic respiration in mice by inhibition of mitochondrial complex IV, again drawing striking parallels to observed H_2S activities in similar systems.[15] A significant limitation to advancing our understanding of the potential roles of H_2Se in biology, however, is the lack of suitable methods for studying H_2Se directly in living systems, although new approaches for both donor and probe technology are beginning to emerge.[19−22]

To expand our basic understanding of differences in the bio(in)organic chemistry between reactive sulfur and selenium species, we recently reported a hydrolysis-based H_2Se donor based on the P═Se motif. By modifying the widely used P═S-containing H_2S donor GYY4137, we prepared the analogous P═Se-containing compound TDN1042 and demonstrated that it releases H_2Se upon hydrolysis by ^{31}P and ^{77}Se NMR spectroscopy as well as H_2Se-trapping experiments.[19] Building from this work, here we report second-generation H_2Se donors that allow for modified H_2Se release rates. To further bridge the gap to using these H_2Se-releasing compounds in biological settings, we use TOF-SIMS (time of flight secondary ion mass spectroscopy) to demonstrate that these donors are cell permeable and result in a dose-dependent increase in intracellular selenium levels. Moreover, we demonstrate that exogenous treatment with the H_2Se donors reduces ROS levels in live cells, which is consistent with antioxidant activity. We anticipate that these results will not only broaden the available chemistry of H_2Se-releasing compounds but also enable future investigations into direct administration of H_2Se in different biological contexts.

RESULTS AND DISCUSSION

Design and Synthesis of Cyclic H_2Se Donors. Although sulfur and selenium are similar main group elements, the inherent reaction chemistry of these elements is often dissimilar. Demonstrating that design approaches for hydrolysis-based H_2S donors can be translated to develop H_2Se donors provides an important step toward advancing and expanding investigations into H_2Se and RSeS in biology. One limitation of the initial TDN1042 system was that H_2Se release was quite slow. To improve on this system and expand the palette of P═Se-based H_2Se donors, we diversified the P═Se platform to investigate how structural modifications impact H_2Se release rates and to compare how these modifications align with known structure−function activities in P═S-based systems.[23] We modified TDN1042 by incorporating *ortho*-substituted phenols that coordinate in a bidentate fashion to the phosphorus center and result in a donor with a single P═Se motif. These donors were prepared by treating Woollins' reagent ($P_2Se_4Ph_2$) with catechol- and 2-aminophenol-based reagents.[24,25] Briefly, refluxing Woollins' reagent with 3 equiv of the desired phenol under N_2 results in formation of the corresponding malodorous cyclized products that can then be purified by silica gel chromatography to afford Cat-PSe (catechol), 2AP-PSe (2-aminophenol), and NMe2AP-PSe (*N*-methyl-2-aminophenol) in low to moderate yields (Figure 2). Each compound was characterized by ^{1}H, ^{13}C, ^{31}P, and ^{77}Se NMR spectroscopy as well as mass spectrometry. The P═Se motif is readily identifiable as a doublet in the ^{77}Se NMR spectrum and as a singlet in the ^{31}P NMR spectrum with characteristic ^{77}Se satellites.

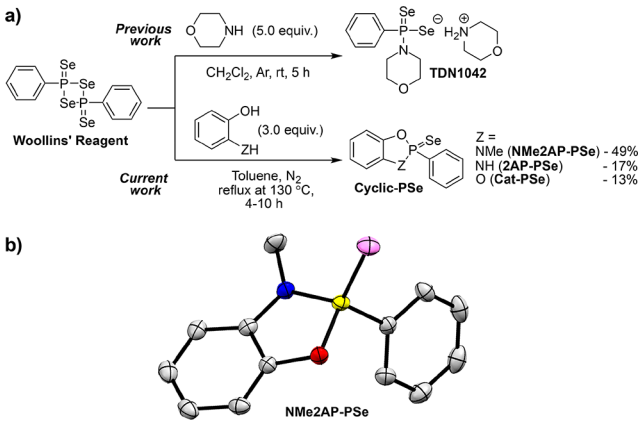

Figure 2. (a) Synthesis of TDN1042 and cyclic-PSe H_2Se donors. (b) ORTEP diagram of NMe2AP-PSe showing 50% probability ellipsoids. Hydrogen atoms are omitted for clarity.

P═Se Hydrolysis and H_2Se Release. With cyclized P═Se donor compounds in hand, we next used ^{31}P NMR spectroscopy to monitor donor hydrolysis in pH 7.4 PIPES buffer. Under these reaction conditions, H_2Se release is accompanied by generation of the corresponding phosphine oxide, which is ultimately hydrolyzed to generate phenylphosphonic acid (PPA). In the case of Cat-PSe, addition to aqueous buffer immediately resulted in the formation of an intermediate that was shifted ∼50 ppm upfield in the ^{31}P NMR spectrum (Figure 3, red square). We attribute this signal to a five-coordinate phosphorus species with P−OH and P−Se^- motifs that is formed by attack of water at the phosphorus center. Subsequent protonation of the anionic selenide leads to rapid extrusion of H_2Se/HSe^- (pK_a = 3.9) with concomitant P═O bond formation.

We also investigated the hydrolysis of 2AP-PSe and NMe2AP-PSe and compared the k_{obs} hydrolysis rates. Our initial hypothesis was that the rate of hydrolysis would depend primarily on the electronegativity of the atoms surrounding the

https://doi.org/10.1021/jacs.1c09525
J. Am. Chem. Soc. 2021, 143, 19542−19550

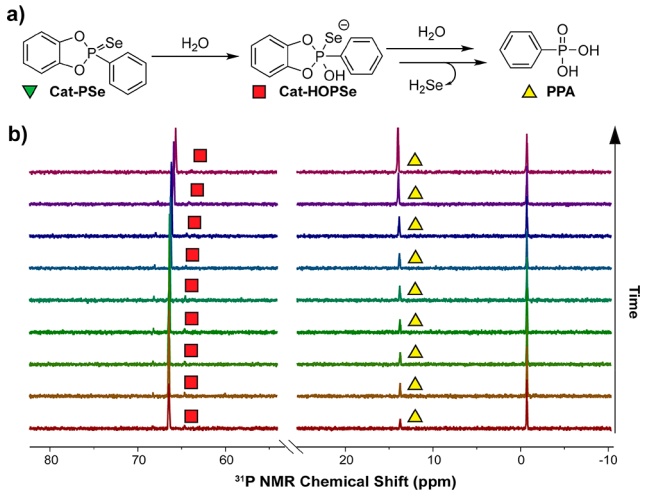

Figure 3. (a) Hydrolysis of Cat-PSe to release H_2Se. (b) Stacked ^{31}P NMR spectra of Cat-PSe (10 mM) hydrolysis in PIPES buffer (pH 7.4, 100 mM) over 450 h at 25 °C.

phosphorus center, with a more electropositive phosphorus center leading to faster hydrolysis rates. This trend, however, was not observed, which suggests that electronic effects are not the primary contributor to donor hydrolysis (Figure 4). For

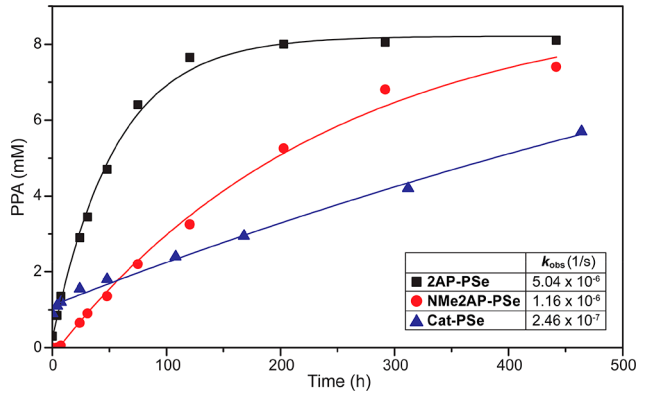

Figure 4. Plotted hydrolysis data (10 mM donor in PIPES 7.4, 100 mM buffer with 5 mM TEP standard at 25 °C) based on the concentration of PPA with tabulated observed rate constants.

example, we expected that the presence of two aryl P−O bonds in Cat-PSe would result in the most electrophilic phosphorus center, but Cat-PSe displays the slowest hydrolysis rate. The 2-aminophenol-based donors, however, did follow the expected trend, with the *N*-methylated donor (NMe2AP-PSe) releasing H_2Se more slowly than 2AP-PSe. One contributing factor to the faster hydrolysis rates of the aminophenol-based donors is the differential bond strength between the weaker aryl P−O bond (141 kcal/mol) when compared to the stronger aryl P−N bond (148 kcal/mol). These small structural changes, when comparing the Cat-PSe and 2AP-PSe donors, result in almost an order of magnitude increase in the rate of donor hydrolysis. Taken together, these data reflect the tunability of P═Se bond hydrolysis based on the structure of the H_2Se donor core.

Mechanistic Studies with ^{31}P and ^{77}Se NMR Spectroscopy. To further investigate the hydrolysis mechanism for the cyclic-PSe compounds and to confirm H_2Se release, we performed alkylative trapping experiments with benzyl bromide (BnBr). These experiments are useful for monitoring selenide release by generating stable, alkylated products, whereas direct H_2Se release often results in selenium autoxidation. Conveniently, these experiments can be followed by ^{1}H, ^{31}P, and ^{77}Se NMR spectroscopy, all of which help to inform on intermediate structures in solution based on the observed heteronuclear coupling constants and multiplicities. Representative NMR spectra for 2AP-PSe are shown in Figure 5, and similar results were observed for the other donors (see SI, Figures S16 and S17 for Cat-PSe and NMe2AP-PSe, respectively).

To simplify the reaction conditions, we performed these experiments in THF-d_8 with 62 mM donor, 124 mM BnBr, and 2.33 M (35 equiv) of water. Under these reaction conditions, attack by water on the phosphorus center breaks the 2-aminophenol chelate to form a four-coordinate P−N intermediate (**1**). This step results in an upfield shift in both the ^{31}P and ^{77}Se NMR spectra and a decrease in the J^1_{P-Se} from 899 Hz to 823 Hz. The identity of this intermediate is supported by the independent synthesis and isolation of the analogous methoxylated species, which showed similar spectroscopic properties including ^{31}P and ^{77}Se chemical shifts of 72 and −212 ppm, respectively, and a J^1_{P-Se} value of 817 Hz (see SI, Figure S18 for X-ray structure). In the absence of an electrophilic alkylating trap, intermediate **1** would be protonated prior to subsequent H_2Se release. Analogously, in the presence of BnBr, intermediate **1** is alkylated to form intermediate **2**, which is supported by the upfield shift of the ^{31}P NMR signal to 27 ppm and downfield shift of the ^{77}Se NMR signal to 300 ppm. Notably, the ^{77}Se signal appears as a doublet of triplets due to coupling to the phosphorus center and the benzyl CH_2 motif (J^1_{P-Se} = 384 Hz, J^2_{Se-H} = 7.1 Hz). Hydrolysis of **2** liberates benzyl selenol (BnSeH), as evidenced by the new resonance in the ^{77}Se spectrum at 78 ppm (dt, J^1_{Se-H} = 42.4 Hz, J^2_{Se-H} = 12.5 Hz). Selenol **2** is subsequently oxidized to form dibenzyl diselenide (Bn_2Se_2), which is characterized by a triplet at 400 ppm in the ^{77}Se NMR spectrum (J^2_{Se-H} = 14.0 Hz). Under these reaction conditions, the autoxidized Bn_2Se_2 is the major product, but dibenzyl selenide (Bn_2Se) is also formed upon reaction of BnSeH with BnBr, which is characterized by a pentet at 330 ppm in the ^{77}Se NMR spectrum. The resultant phosphorus byproduct (**3**) does not accumulate in the reaction mixture and is rapidly hydrolyzed to PPA, which appears at 14 ppm in the ^{31}P NMR spectrum.

Colorimetric H_2Se Detection. Although NMR spectroscopy provides useful information on the chemical environment and connectivity of the different species formed during H_2Se release, spectroscopic detection of H_2Se using optical methods would aid the future development of H_2Se donors and H_2Se detection. Drawing parallels to work on colorimetric systems commonly used for H_2S trapping, we investigated whether 4-chloro-7-nitrobenzofurazan (NBD-Cl) could be used for colorimetric H_2Se detection. Previously, we demonstrated that NBD-Cl reacts with H_2S to generate NBD-SH, which has a characteristic absorbance at 536 nm and allows for colorimetric H_2S detection.[26] NBD-based electrophiles have been used broadly by many groups to develop both colorimetric and fluorescent reporters for H_2S[27] as well as other small molecules.[28] Building from this basic chemistry, we expected that the electrophilic NBD-Cl would also react with H_2Se to produce a highly colored product that could aid H_2Se detection.

https://doi.org/10.1021/jacs.1c09525
J. Am. Chem. Soc. 2021, 143, 19542−19550

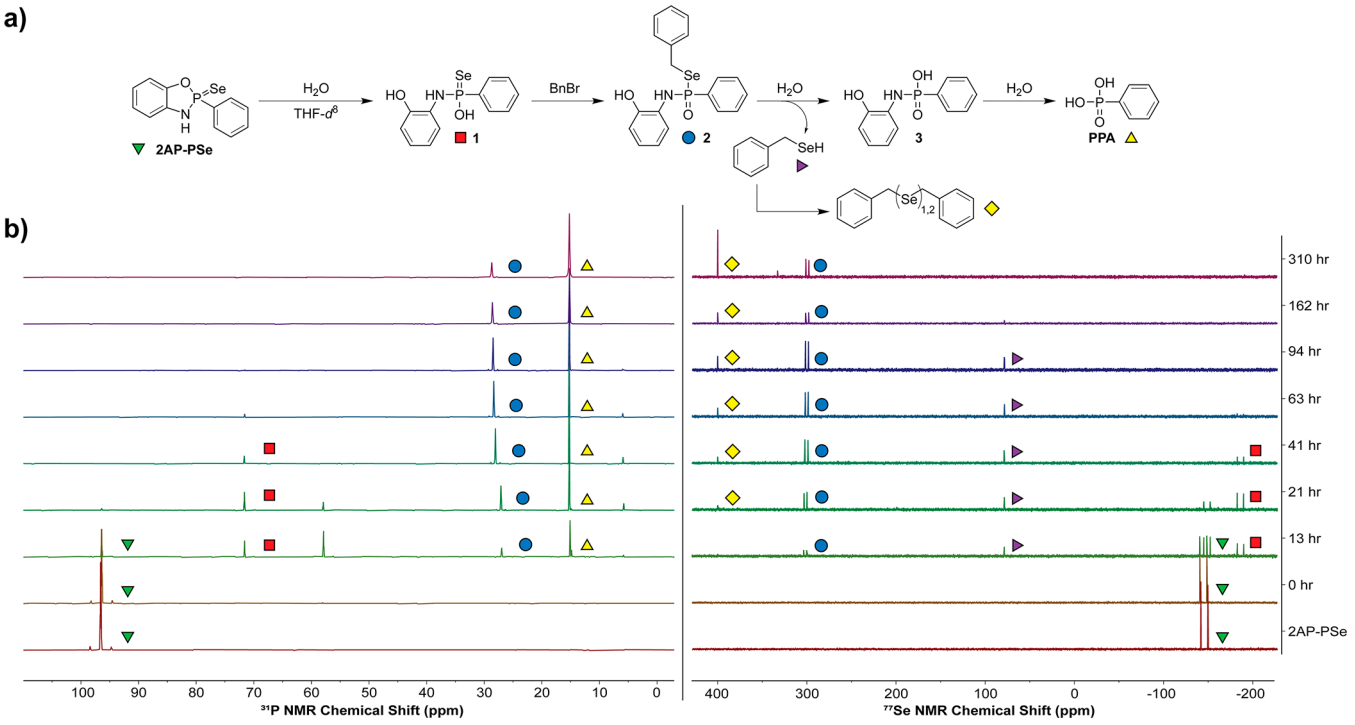

Figure 5. Results of alkylative trapping experiments with BnBr showing (a) the proposed reaction scheme and (b) the corresponding ^{31}P and ^{77}Se NMR data for this reaction (62 mM 2AP-PSe, 124 mM BnBr, and 2.33 M water in THF-d_8 at 25 °C).

To test this chemistry directly, we first treated NBD-Cl with tetrabutylammonium hydroselenide (NBu_4SeH) in pH 7.4 PBS buffer (Figure 6a). When a substoichiometric amount of HSe^- is present with respect to NBD-Cl, NBD_2Se (λ_{max} = 428 nm) is the primary product, which is formed by the intermediate generation of NBD-SeH and subsequent reaction with a second equivalent of NBD-Cl. If stoichiometric HSe^- with respect to NBD-Cl is present, then NBD-SeH (λ_{max} = 551 nm) is the primary product, which forms from either direct reaction of NBD-Cl with HSe^- or the cleavage of the NBD_2Se intermediate with HSe^-. This chemistry can be clearly demonstrated by titrating 0.1 equiv aliquots of NBu_4SeH (10 mM in DMSO) into a solution of NBD-Cl. The intermediate formation of NBD_2Se is observed, which reaches a maximum at 2:1 NBD-Cl:HSe^- stoichiometry, with NBD-SeH being the primary species at a 1:1 NBD-Cl:HSe^- ratio (Figure 6b). The observed absorbance of NBD-SeH at 551 nm is red-shifted from the NDB-SH absorbance at 534 nm, which is consistent with substitution of a heaver chalcogenide. Based on these data, NBD-Cl provides a unique colorimetric response to H_2Se/HSe^- upon formation of the highly colored NBD-SeH product if free H_2Se/HSe^- is present.

In prior unpublished work, we found that attempts to measure H_2Se release from TDN1042 with NBD-Cl resulted in the formation of an unidentified adduct rather than the expected NBD-SeH. In addition, we observed that this reaction was significantly faster than the hydrolysis of TDN1042 (Scheme 1) based on ^{31}P NMR experiments. Because the cyclic-PSe compounds hydrolyze faster than TDN1042, we wanted to further investigate this reactivity and determine whether NBD-Cl could be used to monitor H_2Se release. To test this system initially, we added Cat-PSe (1.0 equiv) to a solution of NBD-Cl (66 μM in PBS 7.4 buffer) and observed the expected formation of NBD-SeH (λ = 551 nm), which is consistent with H_2Se generation (Figure 6c). When comparing

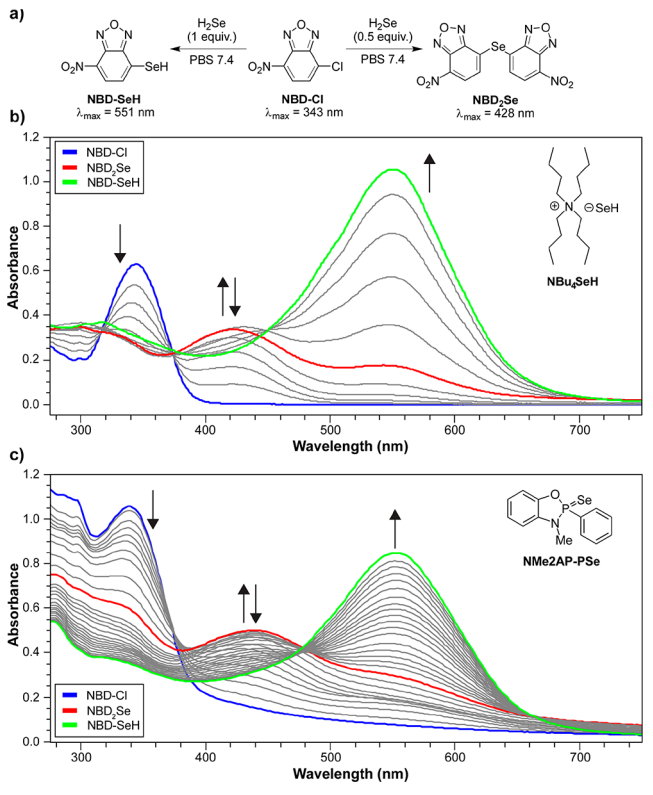

Figure 6. (a) Addition of 1.0 equiv of H_2Se to NBD-Cl results in the direct formation of NBD-SeH. Addition of 0.5 equiv of H_2Se to NBD-Cl results in the formation of NBD_2Se, which can react further with H_2Se to generate NBD-SeH. (b) Titration of NBD-Cl (66 μM in PBS 7.4 buffer) with NBu_4SeH (10 mM in DMSO) in 0.1 equiv increments at 25 °C. (c) Treatment of NBD-Cl (66 μM in PBS 7.4 buffer) with NMe2AP-PSe (1.5 equiv, 99 μM from a 10 mM solution in THF) at 25 °C forms NBD-SeH.

https://doi.org/10.1021/jacs.1c09525
J. Am. Chem. Soc. 2021, 143, 19542−19550

Scheme 1. Proposed Reaction Pathways for the Reaction of (a) TDN1042 and (b) Cyclic-PSe Compounds with NBD-Cl

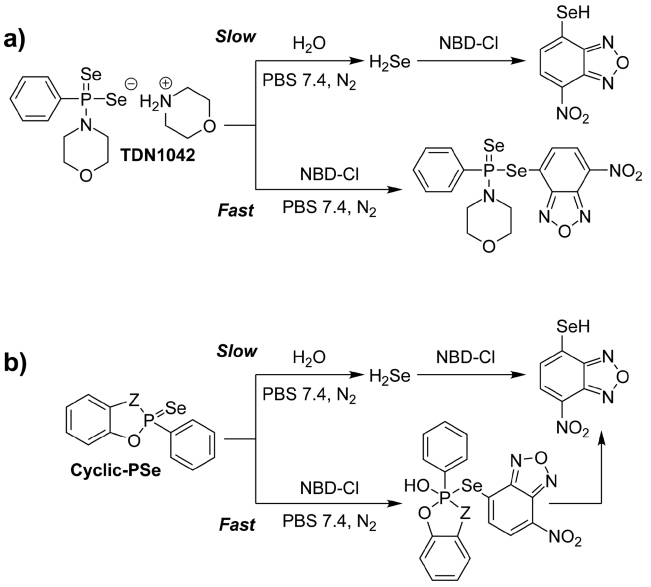

this UV−vis data to ^{31}P NMR hydrolysis experiments, however, we noted a significant difference in rate, with complete hydrolysis occurring in hours as opposed to days. This difference suggests that the presence of a strong electrophile, such as NBD-Cl, results in initial alkylation rather than hydrolysis. On the basis of these rate differences, we propose that the cyclic-PSe compounds react directly with NBD-Cl to form an intermediate that facilitates the subsequent liberation of selenide and NBD-SeH formation. Although the NBD-Cl trapping system confirms that these donors are a source of labile reduced Se, we caution other researchers that NBD-Cl trapping experiments should be complemented with other measurements for RSeS-releasing compounds to not inadvertently interpret direct donor alkylation as alkylation of released H_2Se in solution.[29]

Cell Permeability Studies Using TOF-SIMS. Because H_2Se delivery strategies are only beginning to emerge, little is known about the biocompatibility of these RSeS donors. To help bridge the gap between H_2Se donor development and applications to biological systems, we first focused on determining whether the prepared donors are cell permeable. To achieve this goal, we used TOF-SIMS to measure the concentration of different elements in cells that were treated with donors. This method allows atomic identities to be mapped by monitoring characteristic elemental masses of ionized particles (e.g., Se^- for selenium, PO_3^- for phosphorus). Furthermore, ion beam ablation of the exposed frozen cell surfaces allows for 3D elemental maps to be constructed. Similar approaches based on X-ray fluorescence (XRF) have been used previously to observe cellular localization of Ebselen, a Se-containing glutathione peroxidase (GPx) mimic.[30]

To determine whether H_2Se donors were cell permeable, HeLa cells were grown on silicon chips, incubated with different concentrations of H_2Se donors overnight, fixed with formaldehyde, and measured by TOF-SIMS in depth profiling mode. Cell bodies and peripheral boundaries were identified by mapping the PO_3^- peak. A high level of phosphorus is present throughout the cell and also in the cell membrane phospholipid bilayer (Figure 7ai and bi). To determine

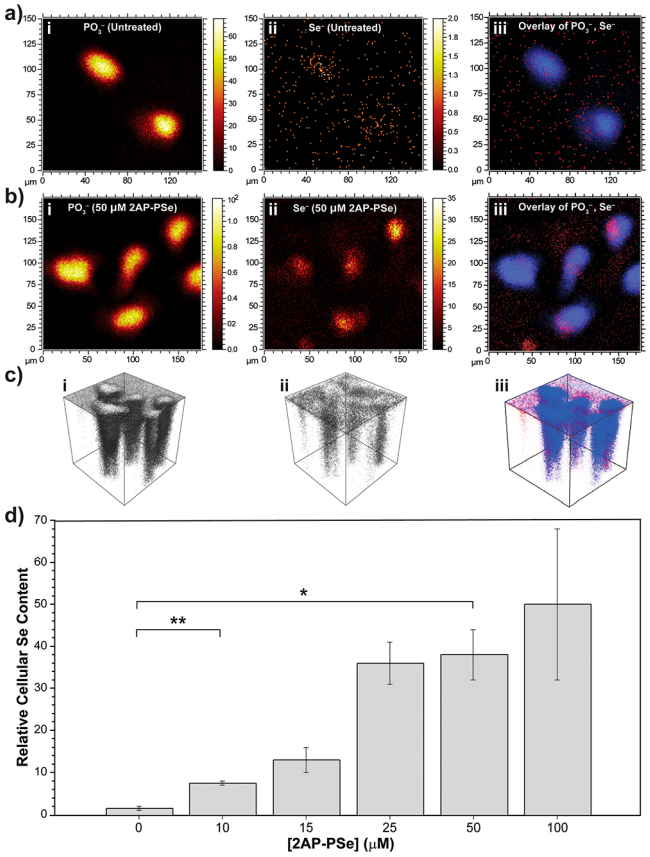

Figure 7. TOF-SIMS images of HeLa cells treated with (a) DMSO (vehicle) showing (i) P, (ii) Se, and (iii) element overlay; (b) 2AP-PSe (50 μM, 18 h) showing (i) P, (ii) Se, and (iii) element overlay. (c) 3D representations of elemental distributions from the data in (b), confirming intracellular localization. (d) Cellular Se content as a function of 2AP-PSe concentration. *$p < 0.05$; **$p < 0.01$ vs control group.

whether the H_2Se donors are cell permeable, we measured the total intracellular Se content as a function of H_2Se donor concentration. If the donors are cell permeable, we would expect to observe a dose-dependent increase in intracellular Se levels on donor treatment. In the absence of H_2Se donors (DMSO vehicle), the HeLa cells showed only trace levels of intracellular Se (Figure 7aii). When treated with 2AP-PSe, significant Se accumulation was observed within the cell boundaries (Figure 7bii). Cell ablation in the z-axis allowed for three-dimensional mapping of intracellular Se, which confirmed that the Se was not solely localized at the cell surface and had been internalized within the cells (Figure 7cii). To further support these conclusions, we also measured the total Se accumulation in HeLa cells with different concentrations of 2AP-PSe (Figure 7d). The Se^- peak intensity detected within the cell boundaries was normalized by the total ion intensity, which allowed us to verify a dose-dependent increase in intracellular Se from 0 to 25 μM, after which the cellular levels plateau. Taken together, the TOF-SIMS data support that these donors can be used to increase intracellular Se levels.

Antioxidant Activity of H_2Se Donors. Having demonstrated that 2AP-PSe can increase intracellular Se levels, we next sought to determine whether 2AP-PSe could exert antioxidant activities in live cells. To probe ROS levels, we used 2′,7′-dichlorofluorescin diacetate (DCFH-DA), a widely used, cell-trappable, fluorescent reactive oxygen species (ROS)

https://doi.org/10.1021/jacs.1c09525
J. Am. Chem. Soc. 2021, 143, 19542−19550

reporter.[31] Upon reaction with ROS such as peroxides, DCFH-DA is oxidized to the highly fluorescent 2′,7′-dichlorofluorescein (DCF, Figure 8a). Our expectation was that pretreatment of cells with 2AP-PSe would provide greater antioxidant activity toward exogenous ROS, which could be monitored directly by DCFH-DA.

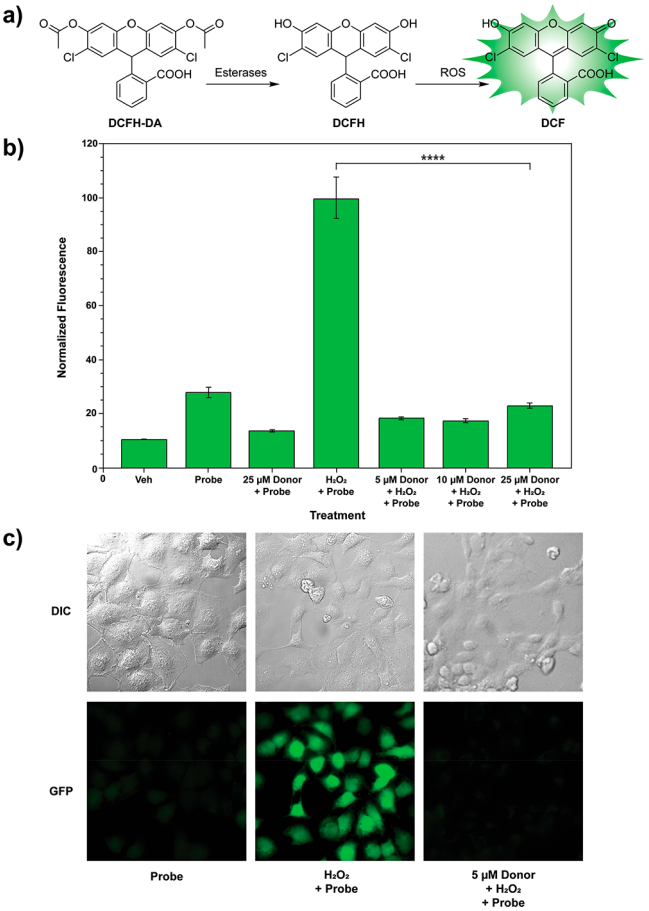

Figure 8. Demonstrated antioxidant activity of 2AP-PSe on HeLa cells as measured by (a) dichlorofluorescein diacetate (DCFH-DA) reacting with ROS, where a major decrease in fluorescence is detected in (b) when the H_2Se donor is applied; probe, DCFH-DA, 5 μM; donor, 2AP-PSe, 24 h incubation; H_2O_2, 500 μM, 30 min incubation; ****$p < 0.0001$ vs control group. (c) Images of cells under the listed treatment conditions on DIC and GFP channels.

To test this antioxidant activity directly, HeLa cells were treated with 5−25 μM 2AP-PSe for 20 h prior to treatment with 5 μM DCFH-DA for 30 min. Cells were washed with buffer and subsequently treated with 500 μM H_2O_2 for 30 min. When compared to background cellular autofluorescence, addition of DCFH-DA resulted in a small fluorescence increase due to endogenous ROS. Addition of 25 μM 2AP-PSe, however, decreased DCF formation, which suggests that 2AP-PSe exerts antioxidant effects on cells. To determine whether 2AP-PSe could be used to provide protection against exogenous ROS, we treated HeLa cells with H_2O_2 and monitored the DCF fluorescence response. Treatment of cells with 500 μM H_2O_2 in the absence of 2AP-PSe resulted in a significant fluorescence response. As expected, pretreatment of cells with 5, 10, or 25 μM 2AP-PSe significantly reduced DCF formation (Figure 8b). Representative fluorescent images are shown in Figure 8c and show decreased ROS-generated fluorescence in the presence of 2AP-PSe. Based on the high reactivity of H_2Se, it is unlikely that these observed effects are due to a buildup of H_2Se directly, but rather an increase in selenium-containing species that facilitate ROS scavenging. Similarly, it is unlikely that the rate constant for the direct reaction of H_2Se with H_2O_2 would be sufficient to outcompete endogenous sources of ROS-scavenging enzymes. We note that these donor concentrations all generate similar reductions in ROS, which suggests that even the 5 μM is sufficient to generate maximal antioxidant activity. Using a significantly higher, but not physiologically relevant H_2O_2 concentration of 10 mM, we observe a dose-dependent, albeit blunted, decrease in DCF fluorescence (see the SI, Figure S27). Taken together, these data show that 2AP-PSe exerts potent ROS-scavenging activity, which is consistent with the proposed antioxidant activity of selenide-containing compounds.

CONCLUSIONS

This work advances H_2Se donor technology by imparting rate tunability into the hydrolysis of P═Se motifs. Further ^{31}P and ^{77}Se NMR spectroscopic studies utilizing alkylative trapping experiments reveal a general mechanism of action, which is consistent with the proposed mechanism of action. Advancing the biological applications of H_2Se donors, we used TOF-SIMS to demonstrate that 2AP-PSe is cell permeable and increases intracellular Se levels in a dose-dependent manner. In addition, we show that 2AP-PSe can reduce ROS and H_2O_2 levels in live cells, which further supports the antioxidant activity of H_2Se. We anticipate that these as well as future H_2Se donors will significantly advance investigations into the roles of reduced RSeS, including H_2Se, in biological investigations.

EXPERIMENTAL SECTION

Materials and Methods. Reagents were purchased from Sigma-Aldrich, Alfa Aesar, and TCI Chemicals and were used directly as received. Deuterated solvents were purchased from Cambridge Isotope Laboratories and used directly as received, except for THF-d_8, which was distilled over sodium and benzophenone prior to use. NBu_4SeH was prepared as described in the literature.[32] Cat-PSe and 2AP-PSe were prepared as described below, and spectroscopic data match previously reported data.[24] ^1H, $^{13}C\{^1H\}$, ^{31}P, and ^{77}Se NMR spectra were recorded on Bruker 500 and 600 MHz instruments. Chemical shifts are reported relative to residual protic solvent resonances for ^1H and $^{13}C\{^1H\}$ spectra. All air-free manipulations were performed in an inert atmosphere using standard Schlenk techniques or an Innovative Atmospheres N_2-filled glovebox. Fluorescent images were taken on a Leica DMi8 wide-field microscope. Images were analyzed and quantified in ImageJ.

General Synthesis of Cyclic-PSe Compounds. Woollins' reagent (0.32 g, 0.60 mmol) and the desired *o*-substituted phenol (1.8 mmol) were added to a flask with anhydrous toluene (15 mL) in a glovebox. The flask was then attached to a septum-sealed reflux condenser, removed from the glovebox, attached to a N_2 line, and placed in an oil bath at 130 °C to reflux. The reaction was monitored by TLC (general reaction time 4 to 10 h). Upon completion, the reaction mixture was concentrated *in vacuo* to afford a black crust, extracted with CH_2Cl_2, and purified via flash column chromatography (SiO_2, 25% EtOAc/hexanes). The identity of the product was verified by ^1H, $^{13}C\{^1H\}$, ^{31}P, and ^{77}Se NMR spectroscopy. See the SI for NMR spectra.

Cat-PSe: pink powder, 46 mg, 13%. ^1H NMR (600 MHz, $CDCl_3$) δ: 7.89 (m, 2H), 7.62 (td, 1H, J^5_{P-H} = 1.7 Hz, J^3_{H-H} = 7.5 Hz), 7.49 (td, 2H, J^4_{P-H} = 4.3 Hz, J^3_{H-H} = 7.8 Hz), 7.14−7.06 (m, 4H). $^{13}C\{^1H\}$ NMR (151 MHz, $CDCl_3$) δ: 145.8, 134.1, 133.3, 131.2, 128.7, 123.8, 112.8. ^{31}P NMR (241 MHz, $CDCl_3$) δ: 115.6 (t, J^1_{P-Se} =

https://doi.org/10.1021/jacs.1c09525
J. Am. Chem. Soc. 2021, 143, 19542−19550

959 Hz, J^3_{P-H} = 16.0 Hz). ^{77}Se NMR (115 MHz, $CDCl_3$) δ: −177.1 (d, J^1_{P-Se} = 959 Hz).

2AP-PSe: orange-pink powder, 60 mg, 17%. ^{1}H NMR (600 MHz, $CDCl_3$) δ: 7.96 (m, 2H), 7.57 (td, 1H, J^5_{P-H} = 1.7 Hz, J^3_{H-H} = 7.5 Hz), 7.47 (td, 2H, J^4_{P-H} = 4.3 Hz, J^3_{H-H} = 7.8 Hz), 7.05 (d, 1H, J^3_{H-H} = 8.1 Hz), 6.98 (t, 1H, J^3_{H-H} = 8.0 Hz), 6.89 (t, 2H, J^3_{H-H} = 7.7 Hz), 5.24 (s, 1H). ^{13}C{^{1}H} NMR (151 MHz, $CDCl_3$) δ: 146.4, 133.6, 133.2, 131.1, 128.4, 112.7, 111.6. ^{31}P NMR (241 MHz, $CDCl_3$) δ: 97.1 (t, J^1_{P-Se} = 894 Hz, J^3_{P-H} = 16.1 Hz). ^{77}Se NMR (115 MHz, $CDCl_3$) δ: −134.3 (d, J^1_{P-Se} = 894 Hz).

NMe2AP-PSe: pink powder, 181 mg, 49%. ^{1}H NMR (600 MHz, $CDCl_3$) δ: 7.86 (m, 2H), 7.57 (td, 1H, J^5_{P-H} = 1.7 Hz, J^3_{H-H} = 7.5 Hz), 7.47 (td, 2H, J^4_{P-H} = 4.3 Hz, J^3_{H-H} = 7.8 Hz), 7.04 (m, 2H), 6.86 (t, 1H, J^3_{H-H} = 7.90 Hz), 6.74 (d, 1H, J^3_{H-H} = 7.8 Hz), 3.00 (d, 3H, J^3_{P-H} = 11.8 Hz). ^{13}C{^{1}H} NMR (151 MHz, $CDCl_3$) δ: 146.3, 136.5, 135.2, 134.4, 133.3, 131.3, 128.5, 123.4, 120.1, 112.1, 108.6, 28.03. ^{31}P NMR (241 MHz, $CDCl_3$) δ: 103.5 (tq, J^1_{P-Se} = 894 Hz, J^3_{P-H} = 15.3 Hz, J^3_{P-H} = 11.8 Hz). ^{77}Se NMR (115 MHz, $CDCl_3$) δ: −181.5 (d, J^1_{P-Se} = 894 Hz). LRMS (ASAP): calcd for $C_{13}H_{13}NOPSe^+$ $[M + H]^+$ 310.0, found 310.1.

2AP-PSe-OMe. The crude product was treated with methanol (5 mL), after which chromatographic purification according to the general procedure produced the title compound. White powder, 182 mg, 46%. ^{1}H NMR (600 MHz, $CDCl_3$) δ: 7.81 (m, 2H), 7.46 (td, 1H, J^5_{P-H} = 1.7 Hz, J^3_{H-H} = 7.5 Hz), 7.40 (td, 2H, J^4_{P-H} = 4.3 Hz, J^3_{H-H} = 7.8 Hz), 6.80 (m, 3H), 6.64 (m, 1H), 6.12 (s, 1H), 3.84 (d, 3H). ^{13}C{^{1}H} NMR (151 MHz, $CDCl_3$) δ: 145.3, 134.1, 133.2, 132.1, 130.6, 128.7, 127.9, 123.2, 121.1, 119.1, 115.4, 52.4. ^{31}P NMR (241 MHz, $CDCl_3$) δ: 71.9 (m, J^1_{P-Se} = 817 Hz). ^{77}Se NMR (115 MHz, $CDCl_3$) δ: −211.6 (d, J^1_{P-Se} = 817 Hz).

Hydrolysis Studies. Stock solutions of phosphine selenide complexes (60 mM) and triethylphosphate (30 mM) were prepared in tetrahydrofuran (THF) in GC vials in a glovebox. Aliquots of 0.10 mL of each stock solution were added to 0.40 mL of PIPES buffer solution (pH 7.4, 100 mM) in NMR tubes. These NMR tubes were removed from the glovebox with tape-sealed septum caps, and the samples were monitored via ^{31}P NMR spectroscopy with gradient shimming and elongated pulse/relaxation times.

Mechanistic Studies with ^{31}P and ^{77}Se NMR Spectroscopy. In a glovebox, the donor (0.035−0.040 mmol) was dissolved in THF-d_8 (0.50 mL) and charged in an NMR tube, which was then capped with a septum and sealed with electrical tape. Baseline ^{31}P and ^{77}Se NMR spectra of the donor solution were acquired prior to addition of a BnBr stock solution in THF-d_8 (0.10 mL, 2.0 equiv, also prepared in a glovebox) and degassed Millipore water (25 μL, 1.4 mmol) via argon-purged Hamilton syringes. This reaction mixture was shaken and monitored by ^{31}P and ^{77}Se NMR spectroscopy over the course of 2 weeks, revealing the formation and conversion of various intermediates to the final products dibenzyl diselenide (Bn_2Se_2, major) and dibenzyl selenide (Bn_2Se, minor).

Hydrolysis Monitoring with NBD-Cl. A stock solution of tetrabutylammonium hydroselenide (NBu_4SeH, 10 mM in DMSO) and NBD-Cl (10 mM in DMSO) was prepared in a glovebox in GC vials that were sealed with electrical tape. In a separate glovebox specifically for aqueous work, a quartz cuvette with a septum cap was charged with PBS 7.4 buffer (3.0 mL, 10 mM). The solutions and cuvette were transported to a UV−vis spectrometer, and a baseline scan (250−750 nm) was taken before addition of NBD-Cl solution (20 μL for a 66 μM solution in the cuvette) and an additional scan to establish the NBD-Cl baseline. After this scan, NBu_4SeH was titrated into solution (2 μL injections, 0.1 equiv) until spectral changes were no longer evident.

The previous procedure was modified slightly to monitor the hydrolysis of the H_2Se donors. Specifically, stock solutions were prepared in THF (10 mM), and the cuvette was equipped with a stirring flea. Baseline scans were taken as detailed above, but the donor was added as a single injection (30 μL, 1.5 equiv), and the hydrolysis was monitored as the reaction stirred. Scans were taken at 2 nm intervals every 12 s for 30 min or until spectral changes were no longer evident.

Cell Culture. HeLa cells (ATCC) were cultured in DMEM containing phenol red (Gibco) and supplemented with 10% fetal bovine serum (FBS) (VWR) and 1% penicillin−streptomycin (10 000 units/mL penicillin and 10 000 μg/mL streptomycin) (Gibco). Cells were maintained at 37 °C under 5% CO_2.

Cellular Proliferation Assay. HeLa cells were seeded in Nunc 96-well Nunclon Delta plates at 10 000 cells/well under normal culturing conditions. The next day, the media was aspirated off and replaced with FBS-free DMEM containing test compounds in 0.5% DMSO (vehicle). Cells remained with test compounds for 24 h before treatment with Cell Counting Kit-8 (CCK-8, Dojindo Molecular Technologies). Data were normalized to vehicle and pooled.

Cell Treatment with 2AP-PSe: TOF-SIMS Depth Profiling and Imaging. HeLa cells were seeded in a 12-well plate containing p-doped (boron) polished wafers (⟨100⟩ orientation, Czochralski-grown, resistivity around 0.012 ohm/cm^2) and were grown overnight in 10% FBS DMEM. The following day, the media was removed, and the cells were washed (2× FBS-free DMEM), treated with 2AP-PSe (10−100 μM, 0.5% DMSO vehicle) in FBS-free DMEM, and incubated for 18 h. After incubation, media was aspirated off and wafers were rinsed 3× with pH 7.4 PBS and fixed with freshly prepared 3.7% paraformaldehyde (PFA) in Milli-Q water for 15 min at room temperature. After incubation, PFA was aspirated off and wafers were rinsed 3× with PBS, 0.1 M ammonium acetate, and Milli-Q water. TOF-SIMS spectra were acquired with a model IV TOF-SIMS instrument manufactured by ION-TOF GmbH, Münster, Germany, using a 25 kV Bi_3^+ primary ion beam and a 2 kV Cs^+ sputter beam. Typically, three or four cells were in the field of view during the depth profile. The depth profile was acquired until all cellular material was ablated, as determined by following the PO_3^- peak intensity during the profile. Using software provided by the vendor we extracted the spectra from the cellular material and measured the Se^- peak area. The software provided the relevant measure of total ion intensity, which was used for normalization. This protocol allows for comparison of the relative Se content in the cells.

Cell Treatment with 2AP-PSe: ROS Assay with DCFH-DA. HeLa cells were plated in glass-bottom imaging dishes (MatTek) at a density of 100 000 cells per dish and were grown in DMEM under normal conditions overnight. The following day, the media was removed and the cells were washed (2× FBS-free DMEM). After rinsing, cells were incubated with 2AP-PSe (5−100 μM) for 20 h in FBS-free DMEM. After incubation the media containing 2AP-PSe was removed, and the cells were washed (2× FBS-free DMEM). Cells were then treated with DCFH-DA (5 μM, 45 min in serum-free DMEM for 30 min). After incubation, cells were rinsed 2× with serum-free DMEM and then were incubated with H_2O_2 (500 μM, 30 min). Cells were then washed 2× with PBS and imaged in FluoroBrite DMEM (Gibco).

■ ASSOCIATED CONTENT

Supporting Information

The Supporting Information is available free of charge at https://pubs.acs.org/doi/10.1021/jacs.1c09525.

NMR spectra, crystallographic data, additional hydrolysis data, additional mechanistic studies, and the cellular proliferation data (PDF)

Accession Codes

CCDC 2108633−2108634 contain the supplementary crystallographic data for this paper. These data can be obtained free of charge via www.ccdc.cam.ac.uk/data_request/cif, or by emailing data_request@ccdc.cam.ac.uk, or by contacting The Cambridge Crystallographic Data Centre, 12 Union Road, Cambridge CB2 1EZ, UK; fax: +44 1223 336033.

https://doi.org/10.1021/jacs.1c09525
J. Am. Chem. Soc. 2021, 143, 19542−19550

AUTHOR INFORMATION

Corresponding Author

Michael D. Pluth − *Department of Chemistry and Biochemistry, Materials Science Institute, Knight Campus for Accelerating Scientific Impact, Institute of Molecular Biology, University of Oregon, Eugene, Oregon 97403, United States;* orcid.org/0000-0003-3604-653X; Email: pluth@uoregon.edu

Authors

Turner D. Newton − *Department of Chemistry and Biochemistry, Materials Science Institute, Knight Campus for Accelerating Scientific Impact, Institute of Molecular Biology, University of Oregon, Eugene, Oregon 97403, United States*

Sarah G. Bolton − *Department of Chemistry and Biochemistry, Materials Science Institute, Knight Campus for Accelerating Scientific Impact, Institute of Molecular Biology, University of Oregon, Eugene, Oregon 97403, United States*

Arman C. Garcia − *Department of Chemistry and Biochemistry, Materials Science Institute, Knight Campus for Accelerating Scientific Impact, Institute of Molecular Biology, University of Oregon, Eugene, Oregon 97403, United States*

Julie E. Chouinard − *Center for Advanced Materials Characterization in Oregon (CAMCOR), University of Oregon, Eugene, Oregon 97403, United States*

Stephen L. Golledge − *Center for Advanced Materials Characterization in Oregon (CAMCOR), University of Oregon, Eugene, Oregon 97403, United States*

Lev N. Zakharov − *Center for Advanced Materials Characterization in Oregon (CAMCOR), University of Oregon, Eugene, Oregon 97403, United States*

Complete contact information is available at: https://pubs.acs.org/10.1021/jacs.1c09525

Notes

The authors declare no competing financial interest.

ACKNOWLEDGMENTS

This work was supported by the NSF (CHE-2004150 to M.D.P.). S.G.B. was supported by the NIH (T32 GM007759). Microscopy, mass spectrometry, and TOF-SIMS instrumentation was supported by the NSF (CHE-1531189; CHE-1625529; DMR-0216639).

REFERENCES

(1) Hatfield, D. L.; Tsuji, P. A.; Carlson, B. A.; Gladyshev, V. N. Selenium and selenocysteine: roles in cancer, health, and development. *Trends Biochem. Sci.* **2014**, *39* (3), 112−120.

(2) Navarro-Alarcon, M.; Cabrera-Vique, C. Selenium in food and the human body: A review. *Sci. Total Environ.* **2008**, *400* (1−3), 115−141.

(3) McKenzie, R. C.; Rafferty, T. S.; Beckett, G. J. Selenium: An essential element for immune function. *Immunol. Today* **1998**, *19* (8), 342−345.

(4) Letavayova, L.; Vlckova, V.; Brozmanova, J. Selenium: From cancer prevention to DNA damage. *Toxicology* **2006**, *227* (1−2), 1−14.

(5) Chen, J. S. An original discovery: selenium deficiency and Keshan disease (an endemic heart disease). *Asia Pac. J. Clin. Nutr.* **2012**, *21* (3), 320−326.

(6) Muller, D.; Desel, H. Acute selenium poisoning by paradise nuts (Lecythis ollaria). *Hum. Exp. Toxicol.* **2010**, *29* (5), 431−434.

(7) Paton, N. D.; Cantor, A. H.; Pescatore, A. F.; Ford, M. J.; Smith, C. A. The effect of dietary selenium source and level on the uptake of selenium by developing chick embryos. *Poult. Sci.* **2002**, *81* (10), 1548−1554.

(8) Burk, R. F.; Hill, K. E. Regulation of selenium metabolism and transport. *Annu. Rev. Nutr.* **2015**, *35*, 109−134.

(9) Reich, H. J.; Hondal, R. J. Why Nature Chose Selenium. *ACS Chem. Biol.* **2016**, *11* (4), 821−841.

(10) Cupp-Sutton, K. A.; Ashby, M. T. Biological Chemistry of Hydrogen Selenide. *Antioxidants* **2016**, *5* (4), 42−59.

(11) Subburayan, K.; Thayyullathil, F.; Pallichankandy, S.; Cheratta, A. R.; Galadari, S., Superoxide-mediated ferroptosis in human cancer cells induced by sodium selenite *Transl. Oncol.* **2020**, *13* (11).100843

(12) Chen, H. J.; Zhou, J. Effects of Sodium Selenite on Oxidative Damage in the Liver, Kidney and Brain in a Selenite Cataract Rat Model. *Biol. Trace Elem. Res.* **2020**, *197* (2), 533−543.

(13) Tarze, A.; Dauplais, M.; Grigoras, I.; Lazard, M.; Ha-Duong, N. T.; Barbier, F.; Blanquet, S.; Plateau, P. Extracellular production of hydrogen selenide accounts for thiol-assisted toxicity of selenite against Saccharomyces cerevisiae. *J. Biol. Chem.* **2007**, *282* (12), 8759−8767.

(14) Pan, X. H.; Song, X. X.; Wang, C.; Cheng, T. T.; Luan, D. R.; Xu, K. H.; Tang, B. H2Se Induces Reductive Stress in HepG(2) Cells and Activates Cell Autophagy by Regulating the Redox of HMGB1 Protein under Hypoxia. *Theranostics* **2019**, *9* (6), 1794−1808.

(15) Iwata, A.; Morrison, M. L.; Blackwood, J. E.; Roth, M. B. Selenide Targets to Reperfusing Tissue and Protects It From Injury. *Crit. Care Med.* **2015**, *43* (7), 1361−1367.

(16) Szabo, C.; Papapetropoulos, A. Hydrogen sulphide and angiogenesis: mechanisms and applications. *Br. J. Pharmacol.* **2011**, *164* (3), 853−865.

(17) Wang, R. Two's company, three's a crowd: can H_2S be the third endogenous gaseous transmitter? *FASEB J.* **2002**, *16* (13), 1792−1798.

(18) Kuganesan, M.; Samra, K.; Evans, E.; Singer, M.; Dyson, A. Selenium and hydrogen selenide: essential micronutrient and the fourth gasotransmitter? *Intensive Care Med. Exp* **2019**, *7* (1), DOI: 10.1186/s40635-019-0281-y.

(19) Newton, T. D.; Pluth, M. D. Development of a hydrolysis-based small-molecule hydrogen selenide (H_2Se) donor. *Chem. Sci.* **2019**, *10* (46), 10723−10727.

(20) Kharma, A.; Misak, A.; Grman, M.; Brezova, V.; Kurakova, L.; Barath, P.; Jacob, C.; Chovanec, M.; Ondrias, K.; Domínguez-Álvarez, E. Release of Reactive Selenium Species from phthalic selenoanhydride in the presence of hydrogen sulfide and glutathione with implications for cancer research. *New J. Chem.* **2019**, *43*, 11771−11783.

(21) Kong, F. P.; Zhao, Y. H.; Liang, Z. Y.; Liu, X. J.; Pan, X. H.; Luan, D. R.; Xu, K. H.; Tang, B. Highly Selective Fluorescent Probe for Imaging H_2Se in Living Cells and in Vivo Based on the Disulfide Bond. *Anal. Chem.* **2017**, *89* (1), 688−693.

(22) Kong, F. P.; Ge, L. H.; Pan, X. H.; Xu, K. H.; Liu, X. J.; Tang, B. A highly selective near-infrared fluorescent probe for imaging H_2Se in living cells and in vivo. *Chem. Sci.* **2016**, *7* (2), 1051−1056.

(23) Feng, W.; Teo, X. Y.; Novera, W.; Ramanujulu, P. M.; Liang, D.; Huang, D. J.; Moore, P. K.; Deng, L. W.; Dymock, B. W. Discovery of New H_2S Releasing Phosphordithioates and 2,3-Dihydro-2-phenyl-2-sulfanylenebenzo d 1,3,2 oxazaphospholes with Improved Antiproliferative Activity. *J. Med. Chem.* **2015**, *58* (16), 6456−6480.

(24) Bhattacharyya, P.; Slawin, A. M. Z.; Woollins, J. D. {PhP(Se)(mu-Se)}(2) by 1,2-C6H4(EH)(E ' H) (E, E ' = O or NH). X-ray crystal structure of $PhP(Se)(NHC_6H_4NH\text{-}1,2)$. *J. Organomet. Chem.* **2001**, *623* (1−2), 116−119.

(25) Hua, G. X.; Fuller, A. L.; Slawin, A. M. Z.; Woollins, J. D. Novel Five- to Ten-Membered Organoselenium Heterocycles from the Selenation of Aromatic Diols. *Eur. J. Org. Chem.* **2010**, *2010* (13), 2607−2615.

(26) Montoya, L. A.; Pearce, T. F.; Hansen, R. J.; Zakharov, L. N.; Pluth, M. D. Development of Selective Colorimetric Probes for

Hydrogen Sulfide Based on Nucleophilic Aromatic Substitution. *J. Org. Chem.* **2013**, *78* (13), 6550−6557.
(27) Yi, L.; Xi, Z. Thiolysis of NBD-based dyes for colorimetric and fluorescence detection of H_2S and biothiols: design and biological applications. *Org. Biomol. Chem.* **2017**, *15* (18), 3828−3839.
(28) Jiang, C. Y.; Huang, H. J.; Kang, X. Y.; Yang, L.; Xi, Z.; Sun, H. Y.; Pluth, M. D.; Yi, L. NBD-based synthetic probes for sensing small molecules and proteins: design, sensing mechanisms and biological applications. *Chem. Soc. Rev.* **2021**, *50* (13), 7436−7495.
(29) Levinn, C.; Pluth, M., Learning from Our Mistakes: We Have a Scientific and Fiscal Obligation to Publish Failed Results. Nov 09, **2020**. *ChemRxiv*. DOI: 10.26434/chemrxiv.13141283.v1 (accessed 2021−06−06).
(30) Wedding, J. L.; Lai, B.; Vogt, S.; Harris, H. H. Investigation into the intracellular fates, speciation and mode of action of selenium-containing neuroprotective agents using XAS and XFM. *Biochim. Biophys. Acta, Gen. Subj.* **2018**, *1862* (11), 2393−2404.
(31) Myhre, O.; Andersen, J. M.; Aarnes, H.; Fonnum, F. Evaluation of the probes 2′,7′-dichlorofluorescin diacetate, luminol, and lucigenin as indicators of reactive species formation. *Biochem. Pharmacol.* **2003**, *65* (10), 1575−1582.
(32) Fargher, H. A.; Lau, N.; Zakharov, L. N.; Haley, M. M.; Johnson, D. W.; Pluth, M. D. Expanding reversible chalcogenide binding: supramolecular receptors for the hydroselenide (HSe^-) anion. *Chem. Sci.* **2019**, *10* (1), 67−72.

https://doi.org/10.1021/jacs.1c09525
J. Am. Chem. Soc. 2021, 143, 19542−19550